DOI: 10.1002/ejic.200701018

Niobia-Supported Palladium–Manganese Materials: Synthesis and Structural Investigation

Roberta Brayner,[a] Françoise Villain,[b] Leon Gengembre,[c] Souad Ammar,[a] and François Bozon-Verduraz*[a]

Keywords: Palladium / Manganese / Niobia / XAS / CO adsorption

Pd/niobia, Mn/niobia, and bimetallic Pd–Mn/niobia materials, which are catalysts for the total oxidation of ethanal, were prepared by anchoring molecular precursors, $Pd(acac)_2$ and/or $Mn(acac)_2$, on niobia before calcination at 400 °C and reduction by either soft chemical routes in liquid medium (Pd-based samples) or at 600 °C in H_2 (Mn/niobia sample). The structure of the obtained materials was investigated by FTIR spectroscopy of adsorbed CO, transmission electron microscopy, X-ray photoelectron spectroscopy, and extended X-ray absorption fine structure–X-ray absorption near edge spectroscopy. On Mn/niobia, Mn^{2+} is largely predominant, in spite of the high reduction temperature used for this sample, and it is mainly engaged in manganese niobate $MnNb_2O_6$. On Pd/niobia, nanoparticles of palladium metal (mean particle size 2.7 nm) are predominant, with a contribution of Pd^{2+}. The surface structure of Pd–Mn/niobia is rather complex. Palladium is distributed between Pd_3Mn nanoparticles and palladium clusters, and both are partially covered by oxygen atoms, whereas Mn^{2+} ions are engaged in MnO clusters linked to niobia.
(© Wiley-VCH Verlag GmbH & Co. KGaA, 69451 Weinheim, Germany, 2008)

Introduction

Manganese-containing materials have wide applications in metallurgy, dry-cell batteries, and magnetic devices. Applications in the field of catalysis are not numerous, but they are now growing. Restricting to monometallic-supported MnO_x, surface characterization[1,2] as well as the interaction of NH_3 and NO_x[3] have been studied on alumina-supported MnO_x, whereas selective catalytic reduction of NO_x has been investigated on carbon-supported MnO_x[4] and dehydrogenation of 1-butene into 1,3-butadiene explored on MnO_2/zirconia.[5] The nature of the manganese species in these materials is strongly influenced by the preparation methods and the thermal treatments; hence several oxidation states may coexist.

In palladium–manganese catalysts, the "bimetallic" designation may be confusing, as manganese is often present in the +2 or +3 oxidation state and palladium either as Pd^0 or Pd^{2+}. The synergistic effect of Pd and Mn_2O_3 has been reported with regard to the oxidation of CO and CH_4,[6] whereas the activity of alumina-supported PdO_xMnO_y catalysts in formaldehyde/methanol combustion has been reported.[7] Renouprez et al. have performed a detailed study of Pd–Mn silica-supported catalysts prepared from Pd and Mn acetylacetonate *impregnation* by using thermal methods, extended X-ray absorption fine structure (EXAFS), X-ray diffraction, transmission electron microscopy (TEM), infrared (IR) spectroscopy of adsorbed CO and NO, with density functional theory calculations.[8,9] They showed that manganese is mostly present as a thin oxide layer spread on the silica surface, whereas the remaining part is incorporated in Pd–Mn alloy particles surface-enriched in Mn.

Niobium oxide, a wide gap n-type semiconductor,[10] has received growing attention in the field of catalysis as both an active phase and a support.[11,12] It is considered by Uchijima as a typical SMSI (strong metal–support interaction) oxide,[13] and SMSI effects have been reported on palladium/niobia after reduction at 773 K[14] and on Co/niobia model catalysts.[15] Palladium/niobia and palladium/niobia–alumina catalysts have been studied in methane,[16] propane,[17] and toluene[18] combustion, ethylene hydroformylation,[14] and hexa-1,5-diene hydrogenation.[19] Among *bimetallic palladium systems* supported on niobia, Pd–Co[20] and Pd–Cu[21] catalysts have been characterized. Abatement of ethanal, an undesired compound emitted, among others, by automobile exhaust of vehicles using ethanol as a fuel has been recently investigated on niobia-supported Pd, Pd-Cu, and Pd-Au.[22] Monometallic Pd catalysts presented a severe deactivation (conversion drop of 80% within 50 min), whereas addition of Au or Cu limited the deactivation to 50%. The present study is devoted to niobia-supported Pd–Mn catalysts that, to the best of our knowledge, have not yet been studied. Our investigations focus on

[a] ITODYS, UMR-CNRS 7086, Université Paris Diderot, 75251 Paris, France
[b] LCI2M, UMR-CNRS 7071, Université Pierre et Marie Curie, 75252 Paris, France
[c] UCCS, UMR-CNRS 8181, Université des Sciences et Technologies de Lille, 59655 Lille, France
Supporting information for this article is available on the WWW under http://www.eurjic.org or from the author.

 © 2008 Wiley-VCH Verlag GmbH & Co. KGaA, Weinheim

niobia-supported Pd, Mn, and Pd–Mn systems prepared by *anchoring* Pd and Mn acetylacetonates on niobia. Characterization was achieved by XRD, UV/Vis/NIR diffuse reflectance spectroscopy (DRS), IR spectroscopy of adsorbed CO, TEM, X-ray photoelectron spectroscopy (XPS), and X-ray absorption near edge spectroscopy (XANES) –EXAFS to determine the structure of the catalysts, and especially the speciation of Pd and Mn.

Results and Discussion

Investigation of the Precursors

The investigation of the precursors by UV/Vis/NIR DRS has brought some relevant information, particularly for the Pd-based catalysts. This was not possible in the case of manganese-containing samples, as electronic transitions involving Mn^{2+} ions are very weak because they are forbidden by both orbital and spin rules.

The DR spectrum of pure Nb_2O_5 calcined at 400 °C (Figure 1a) is characterized by a strong absorption in the UV range as a result of the interband transition and allows the estimation of the bandgap width to 3.4 eV (absorption threshold near 360 nm).[10]

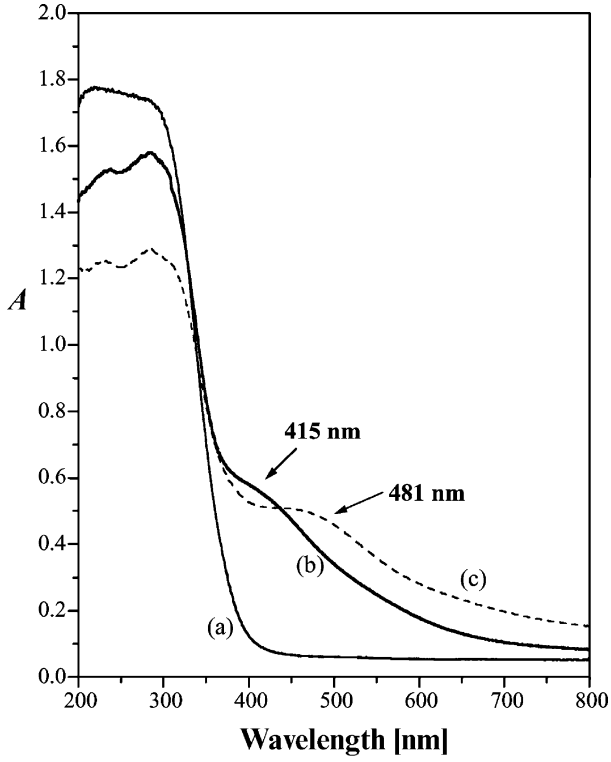

Figure 1. DR spectra of (a) pure niobia calcined at 400 °C; (b) $Pd(acac)_2/Nb_2O_5$ sample after anchoring; (c) PdO/Nb_2O_5 formed by calcination at 400 °C.

The DRS of the $Pd(acac)_2/Nb_2O_5$ sample after anchoring (Figure 1b) shows a shoulder near 415 nm ascribed to the d–d transition of Pd^{2+} and acac ligand charge transfer in $Pd(acac)_2$.[23]

After heating in flowing O_2 at 400 °C, this shoulder is shifted to 481 nm (Figure 1c). This can be ascribed to the formation of isolated Pd^{2+} ions (or to small palladium–oxygen entities) and not to bulk PdO particles, whose absorption threshold lies in the NIR (bandgap width equal to 0.8 eV).[23] EXAFS experiments were conducted on this sample and on bulk PdO. The modulus of the Fourier transforms (FT) of the Pd *K*-edge EXAFS oscillations of the two compounds are compared in Figure 2 (the FTs are presented without phase correction and, as a result, the Fourier peaks are shifted by about 0.3–0.4 Å from the crystallographic distances). Whereas two main peaks appear in the FT of bulk PdO at 1.59 and 2.98 Å, corresponding to the Pd–O and Pd–Pd bonds, only one peak is clearly identified in this *R* range in the FT of the PdO/Nb_2O_5 sample. Its intensity and position are quite similar to those of the Pd–O atomic pair in bulk PdO. Curve-fitting analysis conducted on the corresponding FT^{-1} indicates that the Pd atoms were surrounded by four oxygen atoms at 2.02 Å, such as in bulk PdO. The disappearance of the peak related to the Pd–Pd atomic pair suggests that the produced PdO is highly dispersed over the support, as suggested by DRS. This feature was already observed on oxidized Pd nanoparticles supported on Brönsted acid zeolite (ZSM-5)[24] or alumina.[25] In these cases, a strong interaction with the acid sites of the support favors a high dispersion of PdO. It was already established that Nb_2O_5 prepared according to the Brazilian process has a net Brönsted acid character.[26] Hence, both DRS and EXAFS analyses show that the PdO/Nb_2O_5 sample is constituted of very small palladium–oxygen species (clusters) well dispersed on the acidic support. Hence, the grafting procedure of acetylacetonates appears very convenient for the preparation of very small and well dispersed Pd or Pd-based alloy nanoparticles on niobia, which can be very useful for heterogeneous catalysis.

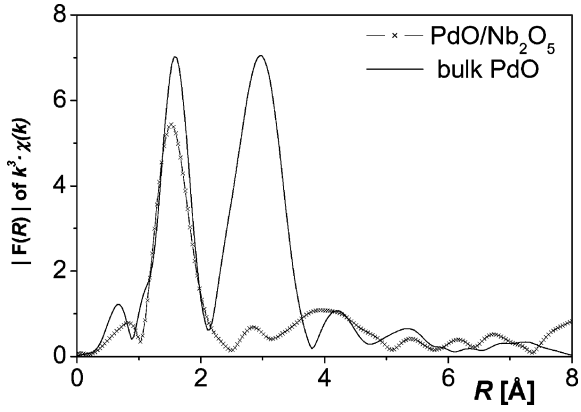

Figure 2. Modulus of the Fourier transforms of the total EXAFS signals of the PdO/Nb_2O_5 sample compared to that of bulk PdO.

Structural Characterization of the Catalysts

The structure and microstructure examination of the three samples, Pd/Nb_2O_5, Mn/Nb_2O_5, and bimetallic Pd–

 © 2008 Wiley-VCH Verlag GmbH & Co. KGaA, Weinheim

Table 1. Characteristics of catalysts.

Sample	Reduction conditions	Measured wt.-% (ICP-AES)		Specific surface area
		Pd	Mn	$[m^2 g^{-1}]$
Nb_2O_5	–			120
Pd/Nb_2O_5	100 °C in ethylene glycol	1.27	–	103
Mn/Nb_2O_5	600 °C under 10%H_2/He stream	–	1.6	20
$Pd–Mn/Nb_2O_5$	80 °C in hydrazine	0.5	0.5	100

Mn/Nb_2O_5, obtained after reduction (Table 1) have been conducted by IRS of adsorbed CO, XPS, TEM, and XANES/EXAFS analysis.

FTIR Spectroscopy of Adsorbed CO

Figure 3 presents the FTIR spectra of CO adsorbed on Pd/Nb_2O_5, Mn/Nb_2O_5, and bimetallic $Pd–Mn/Nb_2O_5$. The spectra were recorded at room temperature under 9 Torr of CO after outgassing at room temperature.

For Pd/Nb_2O_5, CO adsorption gives (i) a peak at 2104 cm^{-1}, which is attributed to linear Pd^0–CO species, possibly with a small contribution of Pd^{2+}–CO; (ii) a broad and intense band centered around 1950 cm^{-1}, ascribed to bridged Pd_2–CO species.[27] Upon evacuation, desorption of linear species is more important than that of bridged ones, and the wavenumber shift to 2085 cm^{-1} attests to the decrease in the dipole–dipole coupling.

For Mn/Nb_2O_5, CO adsorption generates (i) an intense band at 2133 cm^{-1}, assigned to Mn^{2+}–CO;[28] (ii) several weak bands in the 1950–1800 cm^{-1} range. These small bands could at first be ascribed to Mn^0–CO species characterized by a strong back-bonding from manganese to the antibonding π orbitals of CO[29] and consequently resistant to outgassing at room temperature. However, upon outgassing at 20 °C, these bands are markedly weakened and shifted to 2125, 1870, and 1833 cm^{-1}. Hence, they should be assigned to species involving CO weakly bonded to Mn^{2+} (low backbonding).

For $Pd–Mn/Nb_2O_5$, the spectrum presents a strong band at 2140 cm^{-1} with a shoulder around 2109 cm^{-1}, assigned to Mn^{2+}–CO and linear Pd^0–CO, respectively; (ii) a series of weaker peaks and shoulders with maxima in the 2000–1800 cm^{-1} range. After outgassing at 20 °C, the Mn^{2+}–CO species disappear, whereas the most intense band lies at 2109 cm^{-1}, with other peaks at 1958, 1887, and 1820 cm^{-1}. Hence, it appears that the introduction of manganese induces a shift in the Pd^0–CO peak from 2085 (Figure 3a) to 2109 cm^{-1} (Figure 3c), which attests to an *electron-deficiency of palladium atoms*, that is, a partial Pd→Mn electron transfer. This type of interaction may express the formation of a Pd–Mn alloy and is favored in the case of small particles.[30] The bands below 2000 cm^{-1} are assigned to bridged Pd^0 species resistant to outgassing at room temperature. The presence of Mn^0–CO species at the surface is difficult to ascertain because of overlapping with stronger absorption by bridged Pd^0–CO species (Figure 3).

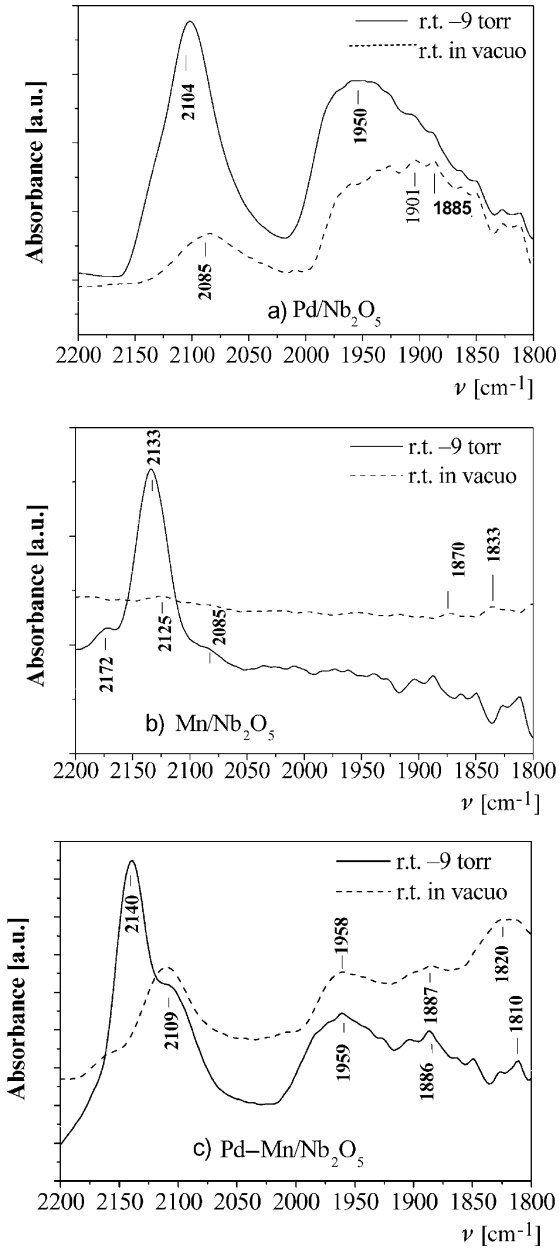

Figure 3. In situ IR spectra of adsorbed CO (P = 9 Torr; T = 25 °C) before and after outgassing of (a) Pd/Nb_2O_5, (b) Mn/Nb_2O_5; (c) $PdMn/Nb_2O_5$.

XPS Studies

The results are collected in Table 2.

 © 2008 Wiley-VCH Verlag GmbH & Co. KGaA, Weinheim

Table 2. XPS experimental binding energies (BE) of mono- and bimetallic samples.

Samples	BE [eV]			
	O1s	$Pd3d_{5/2}$	$Mn2p_{3/2}$	$Nb3d_{5/2}$
Pd/Nb_2O_5	530.4	Pd^0 (335.0)		207.5
Mn/Nb_2O_5	530.3		Mn^{2+} (640.5)	206.5
$Pd–Mn/Nb_2O_5$	530.4	Pd^0 (335.2) Pd^{2+} (337.4)	Mn^{2+} (641.0)	207.5

For Pd/Nb_2O_5, the Nb $3d_{5/2}$ peak is recorded at 207.5 eV, which is close to the value reported in pure niobia,[31] and the O1s line is recorded at 530.4 eV. The $Pd3d_{5/2}$ binding energy (BE) at 335.0 eV is ascribed to Pd^0 species[32,33] in agreement with FTIR spectroscopy.

In the Mn/Nb_2O_5 sample, the Mn $2p_{3/2}$ peak is centered at 640.5 eV. The peak decomposition suggests the predominant presence of Mn^{2+} species (640.5 eV).[34] Whereas the O1s line did not move, the $Nb3d_{5/2}$ BE shifts from 207.5 eV (pure Nb_2O_5 and Pd/Nb_2O_5) to 206.5 eV, which is assigned to the formation of $MnNb_2O_6$ by analogy with the data obtained in niobates.[35] Hence, manganese atoms appear as mainly oxidized, and the diffusion of Mn^{2+} into the support at 600 °C favors the genesis of $MnNb_2O_6$

Finally, for $Pd–Mn/Nb_2O_5$, the position of the Nb $3d_{5/2}$ and O1s peaks are identical to those recorded on Pd/niobia, showing that the manganese ions do not interact strongly with the support in opposition to the Mn/Nb_2O_5 sample. Moreover, the $Pd3d_{5/2}$ BE measured at 335.2 eV and at 337.4 eV (shoulder) correspond to Pd^0 and Pd^{2+} species, respectively.[32] Another peak centered at 641.0 eV is ascribed to Mn^{2+} species. Hence, according to both FTIR spectroscopy and XPS, Pd is present in the 0 and +2 oxidation states with a large predominance of Pd^0 and Mn is present in the +2 oxidation state.

Comparison between bulk and surface Mn/Nb, Mn/(Mn+Nb), and Pd/Nb atomic ratios is presented in Table 3. As expected, the surface Mn/Nb and Mn/(Mn+Nb) ratios are higher. On the other hand, the Pd/Nb surface is slightly lower than the bulk one. This result cannot be ascribed to the presence of large Pd particles as the coordination of Pd in this bimetallic sample is much lower than that in bulk Pd (see below, EXAFS section and Table 4). This implies that all Pd atoms are analyzed by the photoelectrons. According to the simplified Kerkhof–Moulijn morphologic model,[36] the Pd particle size is close to 2 nm.

Table 3. XPS atomic ratios for $Pd–Mn/Nb_2O_5$.

	Global ratio	Surface ratio
n(O)/n(Nb)	2.5	2.35
n(Pd)/n(Nb)	6.1×10^{-3}	5.4×10^{-3}
n(Mn)/n(Nb)	14×10^{-3}	47×10^{-3}
n(Mn)/[n(Mn)+n(Pd)]	0.7	0.9

TEM Observation

The Pd/Nb_2O_5 catalyst was characterized by TEM. The micrographs (Figure 4) show spherical nanoparticles with a size distribution between 1 and 5 nm and an average diameter of d_p = 2.7 nm. The particles appear very well dispersed on the support. Unfortunately, it was not possible to characterize Mn and $Pd–Mn/Nb_2O_5$ materials. This should be due to the weak contrast between manganese and niobium and/or to the small particle size, as suggested by EXAFS data (see below).

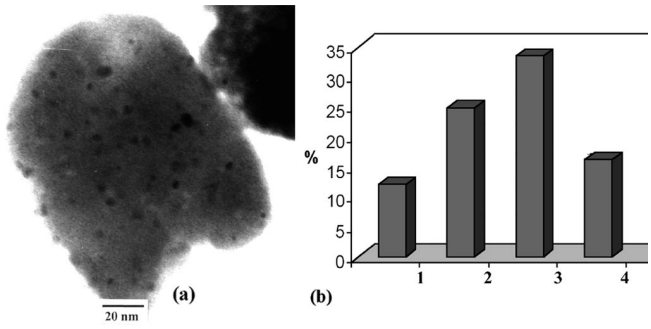

Figure 4. (a) TEM micrograph of Pd/Nb_2O_5 catalyst (the bar scale represents 20 nm); (b) Pd nanoparticle size distribution.

XANES/EXAFS Analysis

XANES and EXAFS experiments were performed at both the Mn and Pd *K*-edges.

For the Pd/Nb_2O_5 sample, the XANES spectrum is compared to that of bulk Pd and PdO in Figure 5. Focusing on

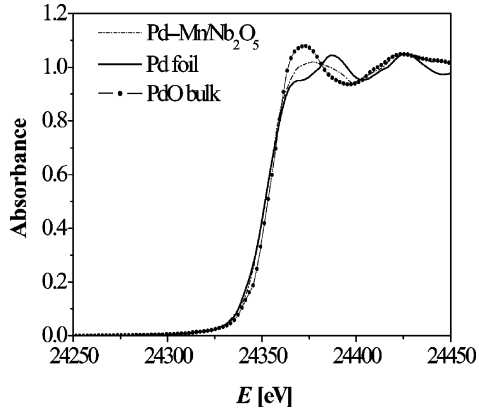

Figure 5. XANES spectra of Pd/Nb_2O_5 and $PdMn/Nb_2O_5$ catalysts compared to those of bulk Pd and PdO.

Table 4. Pd *K*-edge EXAFS results for Pd/Nb_2O_5 and $Pd–Mn/Nb_2O_5$ samples.

Sample	Pair	N	R [Å]	ΔR [Å]	ΔE_0 [eV]	σ [Å]	Residual fit factor [%]
Pd/Nb_2O_5	Pd–Pd	9.0	2.80	1.75–3.10	0.1	0.076	1.3
$PdMn/Nb_2O_5$	Pd–Pd	2.78	2.74	1.80–3.20	4.6	0.05	2.5
	Pd–Mn	0.70	2.78		17.4	0.03	
	Pd–Pd	1.73	2.86		0.3	0.04	

 © 2008 Wiley-VCH Verlag GmbH & Co. KGaA, Weinheim

the edge region, it is possible to confirm that a fraction of palladium atoms is oxidized. The moduli of the Fourier transformation of the total EXAFS signal at the Pd *K*-edge relative to that of bulk Pd and PdO confirms this observation (Figure 6) (FTs are presented without phase correction and, as a result, the Fourier peaks do not correspond exactly to the crystallographic bond lengths of the nearest neighbors). Indeed, the FT of the monometallic catalyst presents a main peak corresponding to the Pd shell. It is at the same distance as that in the FT of bulk Pd, but with a reduced intensity, in agreement with the formation of very small metallic particles. It presents also a peak at a smaller distance, which can be attributed to the Pd–O as located at the distance recorded in bulk PdO. Satisfactory simulations were obtained on the EXAFS oscillations corresponding to the inverse FT filtered in the *R* range 0.95–1.75 Å for the first shell (not shown) and in the 1.75–3.10 Å *R* range for the second shell (Figure 7). They confirm that a part of palladium atoms has almost four first neighbor oxygen atoms at 2.02 Å, whereas another one has nine neighbor Pd atoms at 2.80 Å (in bulk Pd the Pd–Pd distance is 2.758 Å). The results of these simulations are summarized in Table 4.

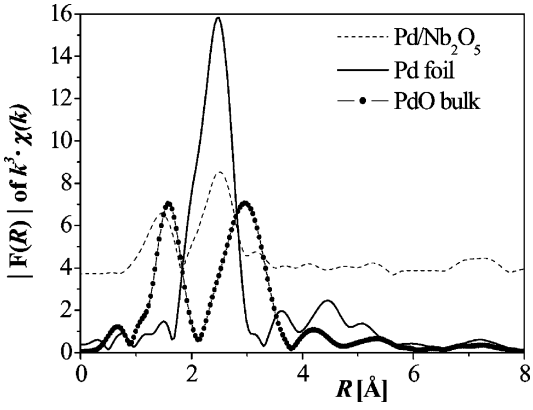

Figure 6. Moduli of the Fourier transforms of the total EXAFS signals of Pd/Nb_2O_5 catalyst compared to those of bulk Pd and PdO.

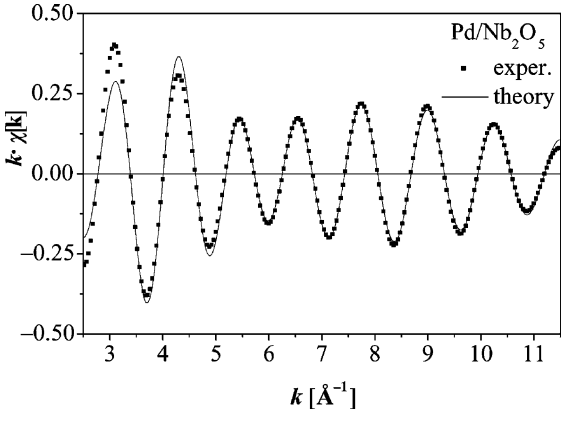

Figure 7. Results of the EXAFS simulation performed on the FT^{-1} metal–metal shell of Pd/Nb_2O_5 at the Pd *K*-edge.

The average number of palladium neighbors obtained with the simulations is smaller for nanoparticles than for the bulk metal.[17] This difference is expected because of the high proportion of atoms located at the surface of the nanoparticles. This number is here slightly smaller than the average number predicted for a naked metal particle. The average number $<N>$ of metal neighbors in a spherical metal cluster can be related to the cluster diameter *D*[37,38] [Equation (1)].

$$<N> = 12–4.79700/D + 0.11352/D^3 \quad (1)$$

For D = 2.7 nm, the expected coordination number $<N>$ is about 10.2. The difference between the calculated values and the experimental one (say 9) suggests that the surface of Pd particles is oxidized, which explains the observation of the Pd–O peak in their FT. Hence, the Pd nanoparticle in the Pd/niobia sample can be described as a metallic core with a diameter slightly smaller than that observed by TEM, surrounded by a surface-oxidized shell. Such a feature has been often observed in metallic nanoparticles prepared by reduction in polyol.[39]

For the Mn/Nb_2O_5 sample, the XANES spectra recorded on the sample and on bulk $MnNb_2O_6$ are very similar (Figure 8), indicating that a large part of Mn interacts with the support to form manganese niobate. Such a feature is confirmed by the perfect superposition of the real and imaginary parts of the FT of the total EXAFS signal recorded at the Mn *K*-edge on Mn/Nb_2O_5 and on bulk $MnNb_2O_6$ (Figure 9). No metallic manganese particles are detected; if any, it should concern a very weak fraction of the initial manganese content. The severe synthesis conditions (heating at 600 °C) favor the diffusion of Mn^{2+} ions into niobia, which thus prevents their reduction by the H_2 flow.

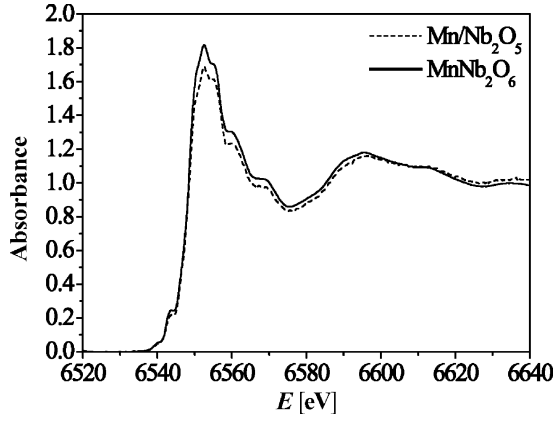

Figure 8. XANES spectrum of Mn/Nb_2O_5 catalyst compared to that of bulk $MnNb_2O_6$.

For the $Pd–Mn/Nb_2O_5$ sample, the XANES spectra recorded at the Pd and Mn *K*-edge are compared to that of (i) bulk Pd and PdO (Figure 10a) and (ii) bulk Mn, $MnNb_2O_6$, and MnO (Figure 10b). At the two edges the spectra are complex. Their shape seems to be intermediate between that of the metal (Pd or Mn) and the oxide (PdO or MnO) references. A complete interpretation of their structure is not possible. However, from the energy differ-

 © 2008 Wiley-VCH Verlag GmbH & Co. KGaA, Weinheim

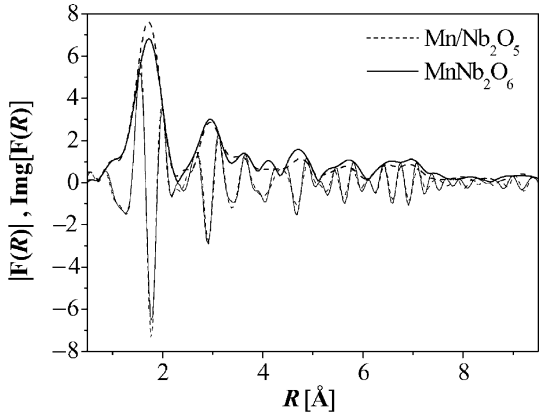

Figure 9. Moduli and imaginary part of the FT of the Mn *K*-edge EXAFS spectra of the Mn/Nb_2O_5 sample and of bulk $MnNb_2O_6$.

ence between the bimetallic sample and the Pd and Mn foils, respectively, it can be concluded that *a minor part of palladium* is in the 2+ valence state, whereas the manganese is almost exclusively in this oxidation state. Comparison of the Pd–Mn/niobia sample with the different metal and oxides references is easier on the zoom on the pre-edge region of the Mn *K*-edge spectra (Figure 10c). It shows a small bump located at 6540.0 eV in both the bimetallic catalyst and the manganese foil, which suggests the presence of a small amount of metallic Mn. This zoom also points out the notable differences existing between the spectra of the bimetallic sample and that of the bulk $MnNb_2O_6$. The shoulder observed in the later compound at 6543 eV (see the arrow) does not exist in the former. Contrary to the monometallic Mn/Nb_2O_5 sample, the manganese does not diffuse into the support as a result of the lowest reduction temperature and possibly the presence of palladium.

At the Pd *K*-edge, the modulus of the FT of the bimetallic sample (Figure 11a) presents a first peak at the low *R* range, ascribed to the Pd–O pairs, followed by a split peak corresponding to the Pd–Pd and/or Pd–Mn pairs. Qualitative comparison between the computed FTs of Pd_3Mn and PdMn cubic alloys and the experimental FT of the sample (Figure 11a) suggests a close structural similitude with Pd_3Mn. Satisfactory simulations were obtained on the EXAFS oscillations corresponding to the inverse FT filtered in the 1.8–3.2 Å *R* range, considering three metal–metal atomic pairs. The quality of the fit is illustrated in Figure 12 and the results summarized in Table 4. It must be noticed that, according to the crystallographic data of Pd_3Mn,[40] there are only two distances (one for Pd–Pd and the other for Pd–Mn) in this *R* range. The first coordination shell of palladium contains eight Pd and four Mn atoms at 2.767 Å, which accounts for the distances obtained on the Pd–Mn/niobia sample, (2.74 Å for the Pd–Pd pairs and 2.78 Å for Pd–Mn). Hence, the Pd–Pd distance at 2.86 Å should be ascribed to the presence of Pd clusters, as already reported on Pd–Mn/silica catalysts.[8,9] Moreover, the refined coordination of palladium is much lower than that expected in such structure. This may be assigned to the high surface/volume ratio (broken symmetry) and to a possible

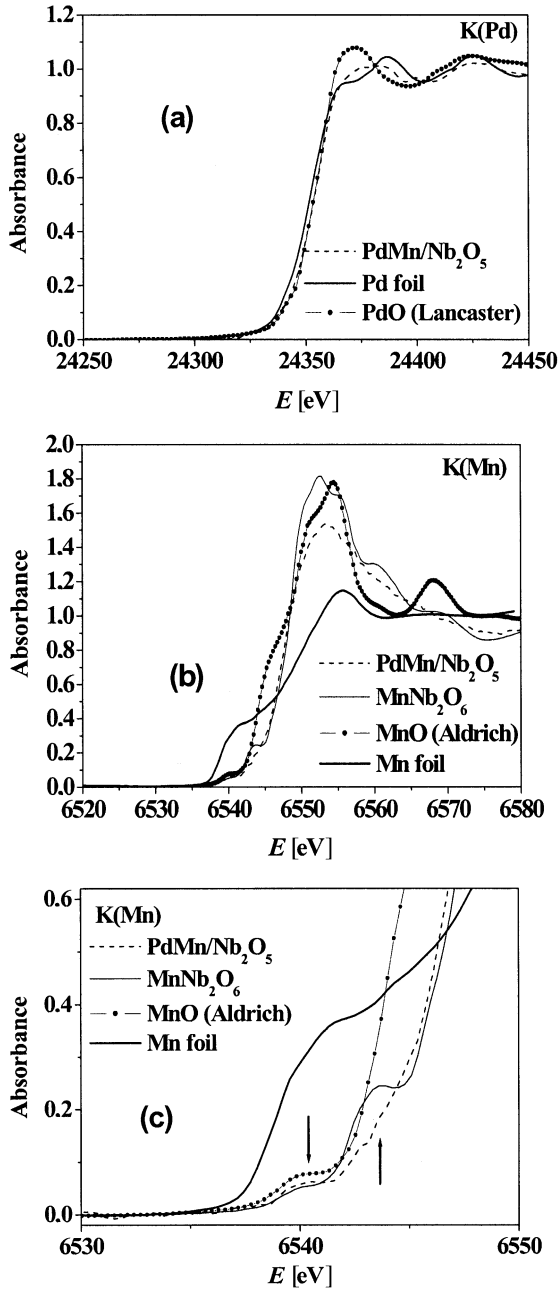

Figure 10. Pd and Mn *K*-edge XANES spectra of $PdMn/Nb_2O_5$ materials compared to those of (a) bulk Pd and PdO and (b) bulk Mn, MnO, and $MnNb_2O_6$; (c) zoom of (b).

surface oxidation. All these results suggest that only a part of introduced palladium and manganese atoms contributes to the Pd_3Mn particles on the niobia surface.

At the Mn *K*-edge (Figure 11b), the FT modulus of the Pd–Mn/niobia sample presents only one distinguishable peak which, by comparison with the FT modulus of bulk Mn, MnO, and $MnNb_2O_6$, can be attributed to the Mn–O atomic pairs. The Mn–Pd and/or Mn–Mn peaks vanish completely. The curve-fitting analysis (not shown), conducted on the corresponding FT^{-1}, is consistent with Mn atoms surrounded by almost three oxygen atoms at 2.13 Å

 © 2008 Wiley-VCH Verlag GmbH & Co. KGaA, Weinheim

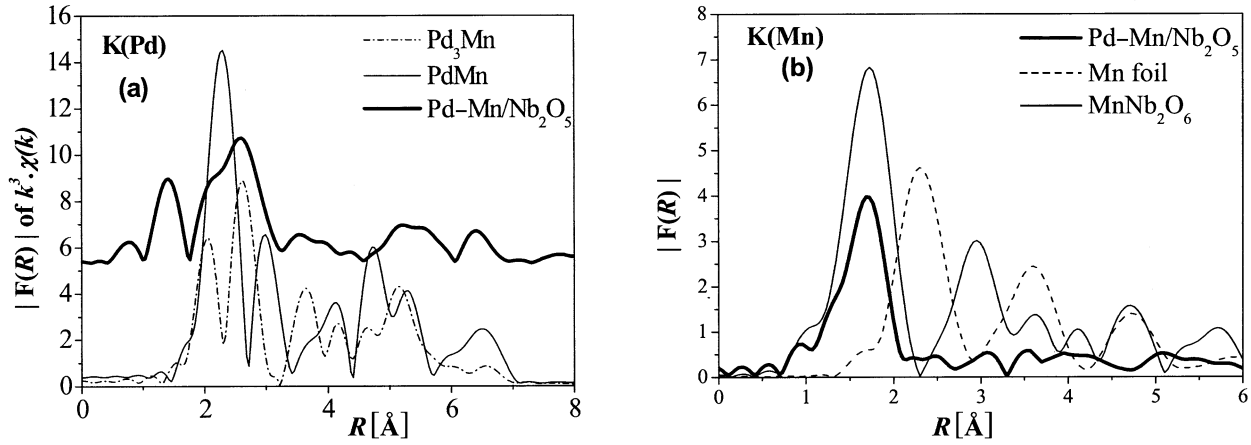

Figure 11. Moduli of the FT of the total EXAFS signal at the Pd and Mn *K*-edge of Pd–Mn/Nb_2O_5 compared to those of (a) Mn, Pd–Mn, Pd_3Mn and (b) bulk Mn and $MnNb_2O_6$.

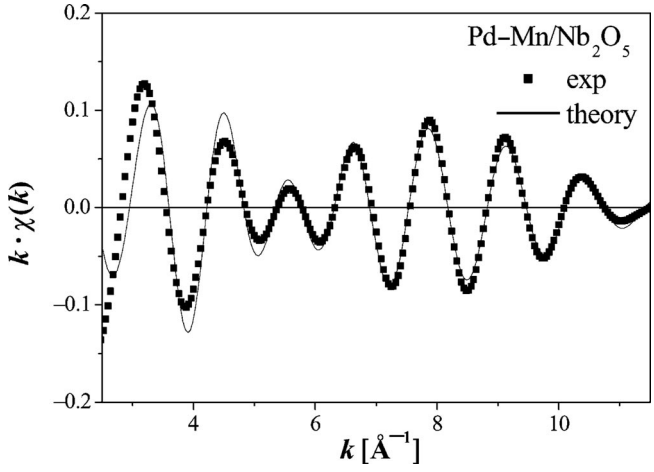

Figure 12. Results of the EXAFS simulation performed on the FT^{-1} metal–metal shell of Pd–Mn/Nb_2O_5 at the Pd *K*-edge.

close to the distances of Mn–O in the cubic MnO oxide, namely 2.22 Å.[41]

The vanishing of the peak related to the Mn–Mn (or Pd–Pd) atomic pairs suggests that the produced MnO is highly dispersed on the support, as previously observed for PdO/Nb_2O_5.

Structural Model Proposed for the Mono- and Bimetallic Catalysts

According to all the spectroscopic techniques performed on the monometallic and bimetallic samples, the following structural models may be proposed.

For Pd/Nb_2O_5, FTIR and XPS analysis show that palladium atoms are mainly in the metallic state Pd^0, with a small contribution of Pd^{2+}. XANES and EXAFS analysis performed at the Pd *K*-edge, confirm the partial oxidation of Pd. The metallic nanoparticles could be surrounded by a PdO-like shell.

For Mn/Nb_2O_5, FTIR analysis suggests that manganese atoms are predominantly in the Mn^{2+}oxidation state. XPS and XAS data show that these Mn^{2+} ions interact strongly with niobia, leading to the formation of $MnNb_2O_6$.

For Pd–Mn/Nb_2O_5, FTIR spectra evidence the presence of Mn^{2+}, with possible traces of Mn^0 and of electron-deficient Pd^0. XPS shows the presence of (i) Pd^0 with a contribution of Pd^{2+}, (ii) Mn^{2+}. The presence of $MnNb_2O_6$, evidenced in Mn/Nb_2O_5, is not detected. The partial oxidation of palladium is also confirmed by EXAFS. It appears that palladium atoms exist (i) in Pd_3Mn particles, (ii) in Pd particles, both probably surrounded by oxidized Pd. The remaining manganese is engaged in MnO clusters partially covering the support.

Conclusions

It is confirmed that the anchoring of Pd acetylacetonate on niobia followed by calcination and reduction in ethylene glycol at 100 °C leads to well-dispersed palladium in Pd/niobia (mean particle size 2.7 nm).

The reduction of Mn^{2+}/niobia at 600 °C under hydrogen is not efficient because the majority of Mn^{2+} is engaged in $MnNb_2O_6$, with a large decrease in surface area (20 $m^2 g^{-1}$ instead of 100 $m^2 g^{-1}$ for Pd/niobia or pure niobia). Hence, a soft reduction process (80 °C in hydrazine) was selected for the synthesis of Pd–Mn/Nb_2O_5 samples to prevent the diffusion of Mn^{2+} in the support and the formation of $MnNb_2O_6$. However, even under these conditions, the reduction of Mn^{2+} to Mn^0 is partial; this can be ascribed to the strong interaction between niobia and oxidized Mn species generated during the calcination. Hence, reduction in hydrazine at 80 °C is able to reduce only a minor part of Mn, which strongly limits the amount available to alloy with Pd. It follows that palladium is mainly engaged in Pd_3Mn species with a Pd to Mn electron transfer, and in Pd clusters, whereas manganese is distributed between Pd_3Mn and Mn^{2+} species identified to MnO.

It is relevant to compare these results with previous data reported on Pd–Mn/silica samples.[8] In this latter case, manganese is distributed between a Pd–Mn alloy and an

 © 2008 Wiley-VCH Verlag GmbH & Co. KGaA, Weinheim

"oxidic form" of Mn, partially covering the alloy particles and the support, even though the reduction temperature was as high as 600 °C. Although the interaction strength between oxidized Mn and silica is weaker than with niobia, reduction at 600 °C is unable to promote the complete reduction of manganese. Hence, the relative interaction strengths of manganese with palladium *and* with the support depend not only on the nature of the carrier but also on the fixation method of the precursors. The anchoring procedure favors the formation of small PdO and MnO clusters on niobia. On the other hand, this advantage is counterbalanced by the lower reduction ability of these species, **w**hich prevents the obtaining of homogeneous supported Pd–Mn materials. The acidity of the carrier may also hinder the reduction of Pd and Mn species.

Following a previous study on Pd/niobia, Pd–Au/niobia, and Pd–Cu/niobia catalysts,[22] tests are now in progress in the total oxidation of ethanal, an undesired compound emitted, among others, by automobile exhaust for vehicles using ethanol as a fuel.

Experimental Section

Catalysts Preparation: Niobia was kindly supplied by CBMM-Brazil (Nb_2O_5-HY-340). $Pd(NO_3)_2$, obtained from Engelhard-CLAL, France, was used to prepare $Pd(acac)_2$; $Mn(acac)_2$ was purchased from Acros and used without further purification.

Anchoring was performed with toluene solutions of $Pd(acac)_2$ or $Mn(acac)_2$.[19] For bimetallic catalysts, the precursors were dissolved simultaneously in toluene. Niobia was then added to the solution and the suspension kept at 50 °C whilst stirring for 2 h. The metal concentrations were chosen by taking into account the anchoring yield, defined as the ratio: quantity of metal anchored on the support/initial quantity of metal in the toluene solution. The solids obtained after filtration were washed with toluene and dried at 50 °C for 12 h. After drying, the anchored samples were calcined at 400 °C under an atmosphere of oxygen (heating rate 0.5 °C min^{-1}) to remove acetylacetonate moieties and generate small PdO particles or clusters. This stage is important because direct reduction of the acetylacetonate complex requires higher temperatures and generates a graphitic layer. After calcination, the samples were reduced according to the following procedures: (i) under a stream of 10%H_2/He at 600 °C (2 h) for Mn/Nb_2O_5; (ii) by soft chemical routes in liquid medium for Pd-based samples, either in ethylene glycol at 100 °C for Pd/Nb_2O_5 or in a hydrazine solution at 80 °C for $Pd–Mn/Nb_2O_5$ to avoid the formation of manganese niobate (see above XPS and XANES results).

The preparation conditions, the metal contents, and the specific surface areas measured after reduction are summarized in Table 1.

Techniques: Chemical analyses were carried out at the CNRS Central Service of Analysis (Vernaison) by inductive coupling plasma-atomic emission spectroscopy (ICP-AES). Transmission electron microscopy (TEM) measurements were performed with a JEOL 100 CXII microscope operating at 100 kV. The particle size distribution was obtained from the TEM pictures by using a digital camera and the SAISAM and TAMIS software (Microvision Instruments), calculating the surface-average particle diameter from [Equation (2)].

$$d_P = \Sigma n_i d_i^2 / \Sigma n_i d_i \quad (2)$$

Transmission infrared spectra were recorded in the 2200–1800 cm^{-1} range with an Equinox 55 Bruker FTIR spectrometer equipped with a DTGS detector. The samples were pressed into self-supporting discs (about 10 mg cm^{-2}) and placed in a stainless steel cell (In situ Research Instruments), allowing in situ analysis of samples in the 20–500 °C range, including CO adsorption. The spectra were taken by averaging 1000 scans, with a scanning velocity of 6.25 Hz and a spectral resolution of 4 cm^{-1} and smoothed through the Savitzky–Golay algorithm with a smoothing degree of 13. Diffuse reflectance spectroscopy (DRS) was performed at room temperature. The spectra were recorded between 190 and 2500 nm with a Varian Cary 5E spectrometer equipped with a double monochromator and an integrating sphere coated with polytetrafluoroethylene (PTFE). PTFE was used as reference. X-ray photoelectron spectroscopy (XPS) analyses were performed with an ESCALAB 220XL spectrometer. The Alk-α monochromatized line (1486.6 eV) was used for excitation with a 200 W applied power, giving a 800 μm spot diameter on the sample. The spectrometer was operated in a constant pass energy mode (Epass = 40 eV) for high-resolution spectra recording by using the electromagnetic lens mode. A 6-eV electron flood gun source was applied to the samples to compensate the charge effect during analysis. Binding energies were referenced to the C1s core level energy at 285 eV for the adventitious carbon species. During the experiment the residual pressure was less than 10^{-7} Pa. Experimental quantification and spectral simulation were obtained by using the Eclipse software provided by VG Scientific. The surface composition of the samples was estimated from XPS peak areas and corrected by the difference in cross section according to Scofield data.[42] X-ray absorption measurements were performed at the French facility (LURE, Orsay) with the XAS 13 beamline of the DCI storage ring (1.85 GeV, position current = 300 mA). For the mono- and bimetallic catalyst samples, X-ray absorption near edge spectroscopy (XANES) and extended X-ray absorption fine structure (EXAFS) experiments were carried out in a fluorescence mode by using, at the Mn *K*-edge, Si (331) double crystal and Si (111) channel-cut monochromators, respectively, and, at the Pd *K*-edge, indifferently Ge (400) double crystal monochromator. Data were also collected in the transmission mode detection scheme (optimized ion chambers) on commercial powder or foil, Mn, MnO (ALDRICH), Mn_2O_3 (ALDRICH), $MnNb_2O_6$ (CERAC), and Pd and PdO (LANCASTER) as standards for Mn and Pd. Data analysis was performed by using the "EXAFS pour le MAC" package.[43] Quantitative single scattering analyses were performed by fitting experimental curves to theoretical models on filtered spectra with the use of the standard EXAFS formula [Equation (3)].

$$k\chi(k) = -S_0^2 \sum_i \frac{N_i}{R_i} |f_i(k, R_i)| e^{-2\sigma_i^2 k^2} e^{\frac{2R_i}{\lambda_i(k)}} \sin[2kR_i + \Phi_i(k, R_i)] \quad (3)$$

where the summation is performed over all the filtered contributions. S_0^2 is the inelastic reduction factor, N_i the number of backscatterers at a distance R_i from the central atom (Mn and Pd respectively), σ_i the Gaussian Debye–Waller factor, and $\lambda_i(k)$ the mean free path of the photoelectron for the backscatterers *i*. Backscattering amplitudes, $|f_i(k, R_i)|$, and phase-shift $\Phi_i(k,R_i)$ functions were calculated from Feff7 code[44] for the different atomic pairs by using the crystallographic data of MnO, PdO, Pd, PdMn (CsCl type),[45] or Pd_3Mn (Cu_3Au type)[40] phases.

 © 2008 Wiley-VCH Verlag GmbH & Co. KGaA, Weinheim

Supporting Information (see footnote on the first page of this article): UV/Vis/NIR spectra of $Pd(acac)_2$/niobia materials before and after calcination are presented.

Acknowledgments

The authors are indebted to CNPq-Brazil for support and financial resources. Thanks are also due to Dr. P. Beaunier for access to TEM equipment.

[1] B. Strohmeier, D. M. Hercules, *J. Phys. Chem.* **1984**, *88*, 4922–4929.
[2] F. Kapteijn, A. D. van Langeveld, J. A. Moulijn, A. Andreini, M. Vuurman, A. M. Turek, J. M. Jehng, I. Wachs, *J. Catal.* **1994**, *150*, 94–104.
[3] F. Kapteijn, L. Singoredio, M. Van Driel, A. Andreïni, J. A. Moulijn, G. Ramis, G. Busca, *J. Catal.* **1994**, *150*, 105–116.
[4] T. Grzybek, J. Klinik, M. Rogoz, H. Papp, *J. Chem. Soc. Faraday Trans.* **1998**, *94*, 2843–2850.
[5] L. A. Boot, M. H. J. V. Kerkhoffs, B. T. van Linden, A. J. van Dillen, J. W. Geus, F. R. van Buren, *Appl. Catal. A* **1996**, *137*, 69–86.
[6] a) Y. Tsuji, S. Imamura, *Stud. Surf. Sci. Catal.* **1993**, *77*, 405–408; b) S. A. Yashnik, Z. R. Ismagilov, V. V. Kuznetsov, V. V. Ushakov, V. A. Rogovand, L. A. Ovsyannikova, *Catal. Today* **2006**, *117*, 525–535; c) V. A. de la Pena O'Shea, M. C. Alvarez-Galvan, J. Requies, V. L. Barrio, P. L. Arias, J. F. Cambra, M. B. Güemez, J. L. G. Fierro, *Catal. Commun.* **2007**, *8*, 1287.
[7] a) M. C. Alvarez-Galvan, B. Pawelec, V. A. de la Pena O'Shea, J. L. G. Fierro, P. L. Arias, *Appl. Catal. B* **2004**, *51*, 83–89; b) V. A. de la Pena O'Shea, M. C. Alvarez-Galvan, J. L. G. Fierro, P. L. Arias, *Appl. Catal. B* **2005**, *57*, 191–199.
[8] A. J. Renouprez, J. F. Trillat, B. Moraweck, J. Massardier, C. Bergeret, *J. Catal.* **1998**, *179*, 390–399.
[9] A. J. Renouprez, J. F. Trillat, C. Bergeret, P. Delichère, J. L. Rousset, J. Massardier, D. Loffreda, D. Simon, F. Delbecq, P. Sautet, *J. Catal.* **2001**, *198*, 243–255.
[10] R. Brayner, F. Bozon-Verduraz, *Phys. Chem. Chem. Phys.* **2003**, *5*, 1457–1466.
[11] E. I. Ko (Ed.), "Catalytic Conversion with Niobium Materials", *Catal. Today* **1990**, *8*(1).
[12] K. Tanabe (Ed.),"Catalytic Properties of Niobium Materials and Related Subjects", *Catal. Today* **1996**, *28*(1–2).
[13] T. Uchijima, *Catal. Today* **1996**, *28*, 105–117.
[14] A. Maeda, F. Yakamawa, K. Kunimori, T. Uchijima, *Catal. Lett.* **1990**, *4*, 107–112.
[15] F. M. T. Mendes, A. Uhl, D. E. Starr, S. Guimondi, M. Schmal, H. Kuhlenbeck, S. K. Shaikhutdinov, H. J. Freund, *Catal. Lett.* **2006**, *111*, 35–41.
[16] M. Schmal, M. Souza, V. Alegre, M. Pereira Da Silva, D. Cesar, C. Perez, *Catal. Today* **2006**, *118*, 392–401.
[17] F. B. Noronha, D. Aranda, A. P. Ordine, M. Schmal, *Catal. Today* **2000**, *57*, 275–282.
[18] K. Okumura, T. Kobayashi, H. Tanaka, M. Niwa, *Appl. Catal. B Environ.* **2003**, *44*, 325–331.
[19] R. Brayner, G. Viau, G. M. Cruz, F. Fiévet-Vincent, F. Fiévet, F. Bozon-Verduraz, *Catal. Today* **2000**, *57*, 187–192.
[20] F. B. Noronha, M. Schmal, B. Moraweck, P. Delichère, M. Brun, F. Villain, R. Frety, *J. Phys. Chem. B* **2000**, *104*, 5478–5485.
[21] F. B. Noronha, M. Schmal, M. Primet, R. Frety, *Appl. Catal.* **1991**, *78*, 125–139.
[22] R. Brayner, D. dos Santos Cunha, F. Bozon-Verduraz, *Catal. Today* **2003**, *78*, 419–432.
[23] A. Rakai, D. Tessier, F. Bozon-Verduraz, *New J. Chem.* **1992**, *16*, 869–875.
[24] a) K. Okumura, J. Amano, M. Niwa, *Chem. Lett.* **1999**, 997–998; b) K. Okumura, J. Amano, N. Yasunobu, M. Niwa, *J. Phys. Chem. B* **2000**, *104*, 1050–1057.
[25] E. Lesage-Rosenberg, G. Vlaic, H. Dexpert, P. Lagarde, E. Freund, *Appl. Catal.* **1986**, *22*, 211–219.
[26] a) K. Tanabe, *Catal. Today* **1990**, *8*, 1; b) T. Ushikubo, T. Iizuka, H. Hattori, K. Tanabe, *Catal. Today* **1993**, *16*, 291–295.
[27] a) N. Sheppard, T. T. Nguyen in *Advances in Infrared and Raman Spectroscopy* (Eds.: R. J. H. Clark, R. E. Hester), Wiley, New York, **1978**, vol. 5, pp. 67–148; b) D. Tessier, A. Rakai, F. Bozon-Verduraz, *J. Chem. Soc. Faraday Trans.* **1992**, *88*, 741–749.
[28] a) M. Kantcheva, M. U. Kucukkal, S. Suzer, *J. Mol. Struct.* **1999**, *482–483*, 19–22; b) M. Kantcheva, M. U. Kucukkal, S. Suzer, *J. Catal.* **2000**, *190*, 144–156.
[29] G. Blyholder, M. V. Allen, *J. Am. Chem. Soc.* **1969**, *91*, 3158–3162.
[30] V. Ponec in *Metal-Support and Metal-Additive Effects in Catalysis*, Elsevier, Amsterdam, **1982**, vol. 11, pp. 63–75.
[31] L. Dragone, P. Moggi, G. Predieri, R. Zanoni, *Appl. Surf. Sci.* **2002**, *187*, 82–88.
[32] D. Briggs, M. P. Seah (Eds.), *Practical Surface Analysis Vol. 1: Auger and X-ray Photoelectron Spectroscopy*, Wiley, New York, **1990**.
[33] F. Bozon-Verduraz, A. Omar, J. Escard, B. Pontvianne, *J. Catal.* **1978**, *53*, 126–134.
[34] a) V. Di Castro, G. Polzonetti, *J. Electron Spectrosc. Relat. Phenom.* **1989**, *48*, 117; b) L. V. Nosova, M. V. Stenin, X. N. Nogin, Y. A. Ryndin, *Appl. Surf. Sci.* **1992**, *55*, 43–48.
[35] M. Kruczek, E. Talik, A. Kania, *Solid State Commun.* **2006**, *137*, 469–472.
[36] V. Leon, *Surf. Sci.* **1995**, *339*, L931–934.
[37] M. Borowski, *J.Phys. IV* **1997**, *7*, C2-259–260.
[38] A. Traverse, *New J. Chem.* **1998**, *22*, 677–683.
[39] N. Chakroune, G. Viau, S. Ammar, L. Poul, D. Veautier, M. M. Chehimi, C. Mangeney, F. Villain, F. Fiévet, *Langmuir* **2005**, *21*, 6788–6796.
[40] H. Iwasaki, K. Okamura, S. Ogawa, *J. Phys. Soc. Jpn.* **1971**, *31*, 497–505.
[41] B. Morosin, *Phys. Rev. B* **1970**, *1*, 236–243.
[42] J. H. Scofield, *J. Electron Spectr. Relat. Phenom.* **1976**, *8*, 129.
[43] A. Michalowicz, *J. Phys. IV* **1997**, *7*, C2-235–236.
[44] J. J. Rehr, J. Mustre de Leon, S. I. Zabinsky, R. C. Albers, *J. Am. Chem. Soc.* **1991**, *113*, 5135–5140.
[45] E. Raub, W. Mahler, *Z. Metallk.* **1954**, *45*, 430–436.

Received: September 20, 2007
Published Online: February 6, 2008

 © 2008 Wiley-VCH Verlag GmbH & Co. KGaA, Weinheim